Proceedings of the ASME 2023 42nd International Conference on Ocean, Offshore and Arctic Engineering
OMAE2023
June 11-16, 2023, Melbourne, Australia

OMAE2023-105048

BUCKLING AND POST-BUCKLING BEHAVIOUR OF EXTRUDED ALUMINIUM PANELS SUBJECT TO THE COMBINED EFFECTS OF WELDING AND PITTING CORROSION

Mojtaba Mokhtari
Centre for Autonomous Marine Operations and Systems (AMOS), Department of Marine Technology, Norwegian University of Science and Technology (NTNU), Trondheim, Norway

Xintong Wang
Centre for Autonomous Marine Operations and Systems (AMOS), Department of Marine Technology, Norwegian University of Science and Technology (NTNU), Trondheim, Norway

Jørgen Amdahl
Centre for Autonomous Marine Operations and Systems (AMOS), Department of Marine Technology, Norwegian University of Science and Technology (NTNU), Trondheim, Norway

ABSTRACT

The present study investigates the effects of pitting corrosion and welding, both independently and combined, on the buckling and post-buckling behaviour of extruded aluminium panels. For this purpose, a finite element model of an aluminium panel made of AA6082-T6 extruded profiles is first developed without having the pitting corrosion and welding effects considered. Then, this finite element model is upgraded to account for the welding effects. This is followed by the validation of the upgraded model against the experimental data obtained from the literature. After the model validation, a hierarchical stochastic algorithm is utilised to simulate the pitting corrosion attack as geometrical defects distributed on the surface of both finite element models, with and without the welding-induced imperfections. Two different corrosion scenarios are considered. In the first scenario, the plating is corroded while the stiffeners remain intact. In the second scenario, the plating is intact, and the stiffeners contain pitting corrosion defects. The corroded parts are modelled with solid, hexahedral elements while shell elements are employed elsewhere. The effect of element type on the numerical results is discussed. Ultimately, the results obtained from the finite element models with and without corrosion and welding effects are compared in terms of ultimate strength, post-buckling response and stress/strain distribution.

Keywords: Aluminium; Buckling; Post-buckling; Ultimate strength; Corrosion; Stochastic algorithm; Welding.

1. INTRODUCTION

Aluminium alloys are increasingly used in marine structures, mainly due to their high strength-to-weight ratio and better corrosion resistance compared to steel. Nevertheless, corrosion is still an issue and corrosion failures have been observed in marine aluminium structures. They often corrode by pitting, one of the most dangerous types of corrosion, rather than uniform corrosion [1]. Pitting corrosion could reduce both the durability and strength of the structure by reducing its effective thickness and promoting stress localization and cracking. Another issue in marine aluminium structures is the sensitivity of aluminium alloys to welding, which causes geometrical and mechanical imperfections.

The ultimate strength of aluminium ship structures with consideration of the welding effects has been extensively studied both experimentally and numerically [2-10]. These studies found that welding could degrade the structural performance of stiffened aluminium panels. The extent of performance deterioration depends on the structure topology, material composition, and welding method. The adverse effects of welding could be curtailed by utilizing extruded panels [11, 12], which require fewer welding paths compared to the traditional built-up panels. However, the literature falls short regarding the evaluation of buckling and post-buckling behaviour of extruded aluminium panels, especially when the welding effects are of concern and corrosion is an issue.

Wang et al. [11] recently investigated the effect of welding on the buckling behaviour of aluminium panels made of AA6082-T6 extruded profiles in a systematic study. In this study, the finite element method (FEM) was employed and the models were validated against the full-scale experiments carried out by Aalberg et al [2]. In these experiments, 21 stiffened aluminium panels, made by welding together extruded profiles with either closed or open (L-shaped) stiffeners, were tested under uniaxial compression loading. The panels were mounted vertically in the test rig with simply supported loading ends as shown in Figure

1. The present study is based upon one of these tests as discussed in the next section.

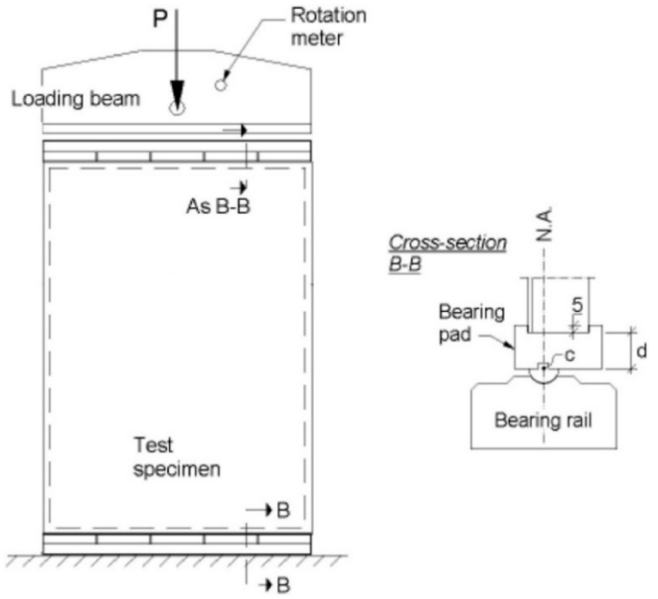

FIGURE 1: SCHEME OF THE EXPERIMENTAL TEST SET-UP IN [2].

For the numerical modelling of pitting corrosion defects in aluminium panels, long-term corrosion data of aluminium alloys are required. There are very few studies that have investigated the long-term corrosion behaviour of aluminium alloys, especially that of the 6xxx series, which are herein of interest. Two studies on this topic found in the open literature are conducted by Liang et al. [13, 14]. In these studies, AA6060-T5 alloy coupons were exposed to marine splash, mean tidal, low tidal and full immersion conditions for 2(+), 3, 3.5 and 4 years. Detailed analyses of pitting corrosion morphologies and characteristics were conducted. The general pitting corrosion morphologies at two different exposure times, shown in Figure 2 [13], are used in the present study as a guide to model the corrosion damage. The models presented herein are based on the mass loss and pit depth data obtained from the 4-year full immersion condition (Table 1).

Despite the great level of irregularities in the morphology of corrosion pits, they are often modelled by overly simplified 2- or 3-dimensional geometries (e.g., circular holes or hemispherical, cylindrical, and conical geometries) in numerical and experimental studies [15-25]. The irregular morphology of pitting corrosion is often caused by the amalgamation of smaller pits that have grown and merged into a bigger pit [26-31]. Secondary pits emerge and grow inside an existing pit leading to the so-called 'pits-within-pits' phenomenon contributing to the surface roughness inside an isolated pit. To model these characteristics of pitting corrosion morphology, Mokhtari and Melchers proposed an algorithm, termed 'hierarchical stochastic algorithm' hereafter, that can more accurately model the isolated pitting corrosion profiles [28-31]. An example of an isolated pit, automatically developed by a Python code of this algorithm linked to Abaqus/CAE [32], is shown in Figure 3. To implement this algorithm for a large surface with many pits, a simplified version of it is adopted in the present study. More details are provided in the methodology section.

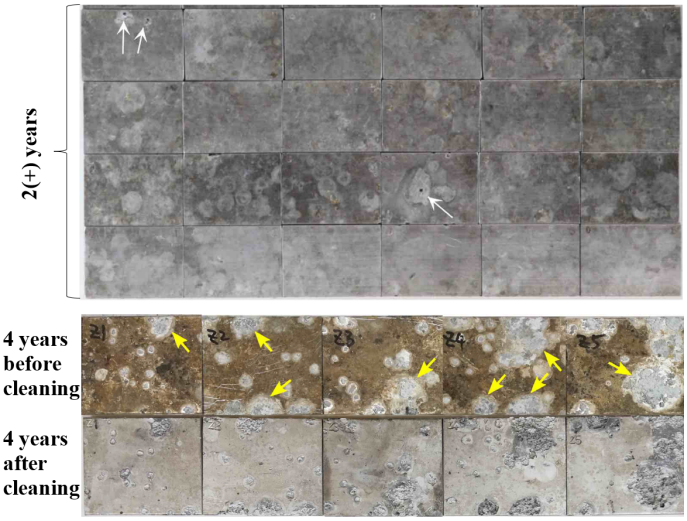

FIGURE 2: OVERALL PITTING CORROSION MORPHOLOGY OF AA6060-T5 COUPONS FOR 2(+) AND 4-YEAR FULL IMMERSION CONDITION [13].

TABLE 1: PITTING CORROSION DATA FOR 4-YEAR FULL IMMERSION OF AA6060-T5 ALLOY IN NATURAL SEAWATER.

Average mass loss (g/m^2)	Max. pit depth (mm)	Average of 15 deepest pits (mm)	Standard deviation (mm)
275.77	2.506	1.525	0.346

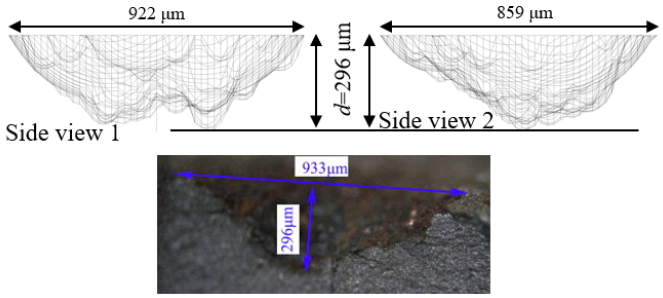

FIGURE 3: MORPHOLOGIES OF A REAL PIT (BOTTOM [33]) AND AN ARTIFICIAL PIT GENERATED AUTOMATICALLY BY THE ORIGINAL HIERARCHICAL STOCHASTIC ALGORITHM (TOP [34]).

Ten different finite element models are developed in this study to investigate the effects of pitting corrosion and welding on the buckling and post-buckling behaviour of extruded aluminium panels. The finite element modelling is explained in the following section. Then, the results are presented with a detailed discussion on the ultimate strength, post-buckling behaviour and stress/strain distribution in the aluminium panel under different corrosion and welding conditions.

2. METHODOLOGY

As mentioned earlier, the co-authors of this study developed a series of finite element models [11] to simulate the experimental buckling tests carried out by Aalberg et al [2]. In these finite element models, developed with Abaqus/CAE v2019 [32], the specimens were modelled using shell elements. One of these models is upgraded in the present study by using a combination of shell and 3D solid elements, where the solid elements are utilized to model the pitting corrosion attack as localised geometrical defects. The model selected for upgrading is shown in Figure 4. This model consists of three extruded AA6082-T6 profiles with the cross-sectional geometry schemed in Figure 5, welded together with metal inert gas (MIG) welding.

The welding introduced mechanical and geometrical imperfections. Mechanical imperfections include residual stresses and reduced strength in the heat affected zone (HAZ). The residual stresses in the plating are 106 MPa in HAZ and −12.6 MPa elsewhere according to the investigations in [11] (the negative sign denotes compressive stress). The residual stresses are applied in the longitudinal direction of the plating (i.e., Z direction).

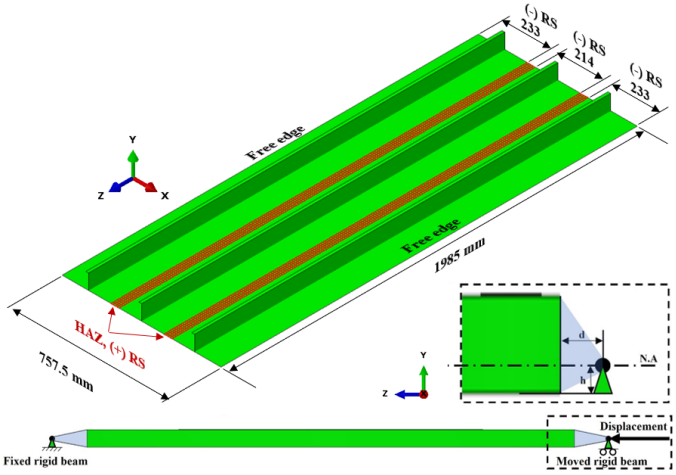

FIGURE 4: DIMENSIONS, HAZ, RESIDUAL STRESS CONDITIONS, AND THE BOUNDARY CONDITIONS OF THE FINITE ELEMENT MODEL. RS STANDS FOR RESIDUAL STRESS, (−) DENOTES COMPRESSIVE STRESS, AND (+) DENOTES TENSILE STRESS.

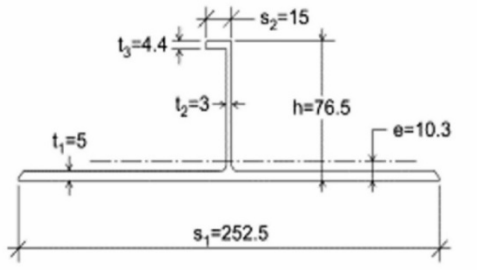

FIGURE 5: CROSS-SECTIONAL GEOMETRY AND DIMENSIONS OF EACH EXTRUDED ALUMINIUM PROFILE [2].

The mechanical behaviour of the panel is modelled using the Ramberg-Osgood relationship expressed as

$$\varepsilon=\frac{\sigma}{E}+0.002\left(\frac{\sigma}{\sigma_y}\right)^n \quad (1)$$

where ε, σ, E, n, and σ_y are strain, stress, Young's modulus, hardening exponent, and the 0.2% offset yield stress. The Ramberg-Osgood parameters for the stiffener and HAZ materials as well as the plating parent material are given in Table 2. Young's modulus and Poisson's ratio are set to 62.61 GPa and 0.33 for all materials in the panel. These are based on the stress-strain curves obtained from the uniaxial tensile tests conducted in [2].

TABLE 2: RAMBERG-OSGOOD MODEL PARAMETERS.

Plating parent material		HAZ		Stiffener	
σ_y (MPa)	n	σ_y (MPa)	n	σ_y (MPa)	n
254	16	152.4	8.51	270	20

The geometrical imperfections are modelled using a single half-sinusoidal wave in the longitudinal direction of the plating and stiffeners. The amplitudes of the sinusoidal waves are taken from the reference study [2]. They resulted from measuring the initial longitudinal bow amplitudes (i.e., in Y direction) of each extruded profile at the midspan of the plating side and initial sideways bow (i.e., in X direction) of the L-shaped stiffeners at the flange tip. The resultant geometrical imperfection fields in X and Y directions are illustrated in Figure 6.

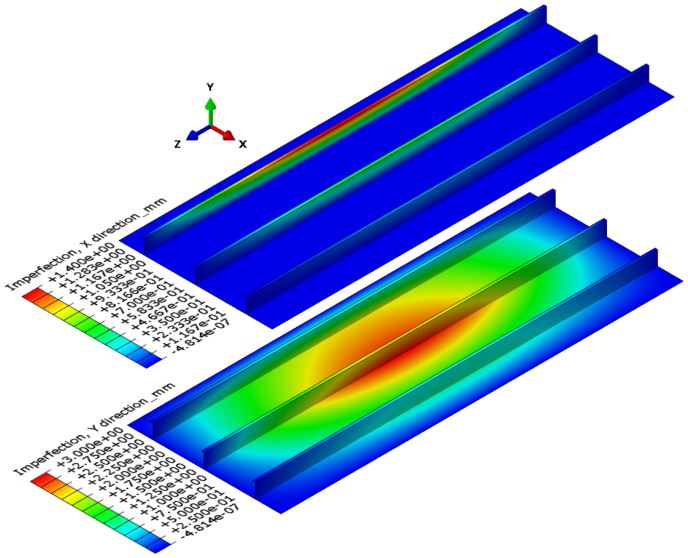

FIGURE 6: GEOMETRICAL IMPERFECTION FIELDS IN THE X AND Y DIRECTIONS.

The bearing systems at the top and bottom ends of the panel in Figure 1 are modelled using rigid beams (see Figure 4). These rigid beams control the movements of the panel nodes at the top and bottom edges of the panel using the kinematic coupling constraint in Abaqus [32]. In Figure 4, the height h and the

distance d are consistent with those in the experimental test [2]. All degrees of freedom of the rigid beams are closed except for rotation about the X-axis. This will provide simply supported boundary conditions. The load is applied by moving one of the beams in the Z direction under displacement-controlled condition. The quasi-static analysis of the dynamic implicit solver of Abaqus was adopted, based on the parametric study performed in [11] that determined the appropriate solver for the problem discussed herein. In the quasi-static analysis, the speed of the moving rigid beam is set to 1.0 mm/minute, which is consistent with the reference experiment.

To model the pitting corrosion attack, a simplified version of the hierarchal stochastic algorithm [28-31] is employed. The algorithm, written in Python and linked with Abaqus/CAE, incrementally cuts spherical caps from the model surface to generate a coalescence of pits in three hierarchical levels. In the first level, large broad pits, also known as 'historical pits', are cut from the intact surface. Pit parameters (i.e., depth, radius, and centre coordinates) follow stochastic distributions. The pit depth is assumed to have a Gaussian distribution with the distribution parameters given in Table 1 while the pit radius and centre coordinates are uniformly distributed. In the second and third levels, smaller and sharper pits with radii downscaled by factors of 1/6 and 1/15, respectively, with respect to the historical pit radii are cut from the corroded surface generated in the first level. This will generate secondary pits inside the existing historical pits. The resultant corroded surface is shown in Figure 7. Although the pit depth in each level could have a probability distribution other than Gaussian such as lognormal or extreme value, they are deemed to have a negligible effect on the results of this study.

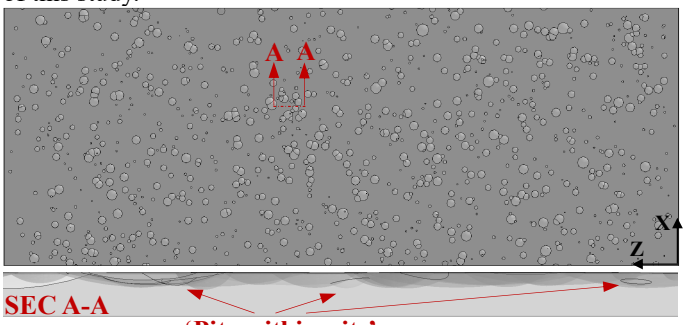

FIGURE 7: THE PLATING WITH PITTING CORROSION DEVELOPED BY A SIMPLIFIED VERSION OF THE HIERARCHICAL STOCHASTIC ALGORITHM IN [30, 31].

Two different scenarios of corroded panels are studied, first a corroded plating with intact stiffeners and second an intact plating with corroded stiffeners. This is to determine the condition under which the panel's structural behaviour is more affected by corrosion. For the first scenario, the corroded plating is modelled with 119200 linear hexahedral elements with reduced integration (C3D8R) while 5400 linear quadrilateral shell elements with reduced integration (S4R) are used to model the intact stiffeners. In the second scenario, two different cases with different solid element types for the stiffeners are considered. In the first case, the intact plating and the corroded stiffeners are modelled with 17910 S4R and 26992 C3D8R elements, respectively. In the second case, the element type of the stiffeners is changed to quadratic with full integration (C3D20) from linear with reduced integration (C3D8R). The reason is discussed in the following section. In both corrosion scenarios, four elements are employed along the thickness of the parts with solid elements. Mesh configurations of the models are shown in Figure 8. The intact counterparts of the corroded models are also developed to compare each corroded case with its intact counterpart. This is to ensure that the conclusions are independent of the element type. To generate these intact models, the nodes of the corroded surface are projected onto the initial intact surface thereby removing the corrosion defects. Subsequently, the mesh configuration of the intact and corroded models is almost the same. Each model is run with and without welding effects. In addition, the original all-shell-element model developed in [11] is also considered in this study to investigate the effect of element type on the results. Altogether, 10 different finite element models are included in the study with the conditions listed in Table 3.

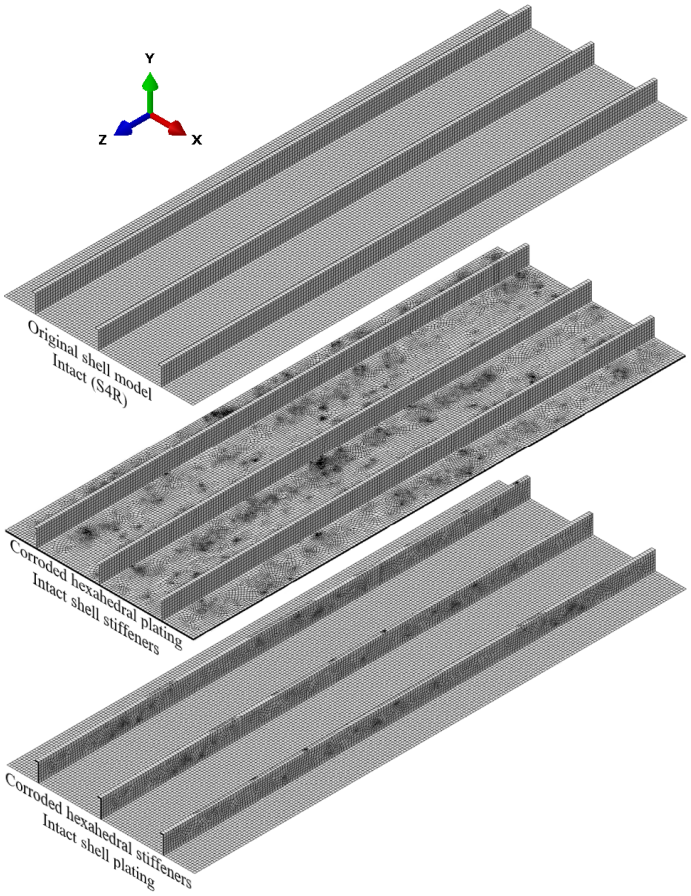

FIGURE 8: THREE DIFFERENT MESH CONFIGURATIONS INCLUDED IN THE STUDY.

TABLE 3: MODEL ABBREVIATIONS AND CONDITIONS.

Model #	Plating condition	Stiffener condition	Plating element type	Stiffener element type	Welding effect
IP-IS-S4S4-W	Intact	Intact	S4R	S4R	Yes
IP-IS-C8S4-W	Intact	Intact	C3D8R	S4R	Yes
CP-IS-C8S4-W	Corroded	Intact	C3D8R	S4R	Yes
IP-IS-C8S4	Intact	Intact	C3D8R	S4R	No
CP-IS-C8S4	Corroded	Intact	C3D8R	S4R	No
IP-IS-S4C8-W	Intact	Intact	S4R	C3D8R	Yes
IP-IS-S4C20-W	Intact	Intact	S4R	C3D20	Yes
IP-CS-S4C20-W	Intact	Corroded	S4R	C3D20	Yes
IP-IS-S4C20	Intact	Intact	S4R	C3D20	No
IP-CS-S4C20	Intact	Corroded	S4R	C3D20	No

3. RESULTS AND DISCUSSION

Figure 9 shows the response curves (i.e., axial load vs. end-shortening) for all the uncorroded models with consideration of the welding effects plotted together with the experimental data. All the curves follow almost the same path up to the ultimate load and exhibit a mostly linear trend. After the critical displacement corresponding to the ultimate load, D_{cr}, the response curves diverge from one another. The response curves by the models with S4R stiffeners drop abruptly and significantly at D_{cr} while the experimental curve shows a smoother reduction of load. This has caused large underestimations of the post-buckling strength by these models with S4R stiffeners. On the other hand, the model with C3D8R stiffeners has overestimated the post-buckling strength. However, the smooth reduction of the response load by this model is more consistent with the experimental data. These findings demonstrate that the numerical results are very sensitive to the element type used for modelling the stiffeners, and hexahedral elements may be better candidates for the stiffeners as opposed to the shell elements. To improve the numerical results while keeping the same mesh configuration, the C3D8R elements of the stiffeners were replaced with C3D20 elements. By doing so, the results have significantly improved although there is still a considerable difference between the numerical and experimental post-buckling response that increases with the axial displacement.

The simulations with S4R stiffeners in Figure 9 took substantial computation effort due to numerical instabilities caused by dynamic stiffener tripping, vibrations and/or other dynamic actions. The time increment dropped below 0.001 and became as small as 10^{-5} for hundreds of increments. Although it is often computationally cheaper to use shell elements in modelling thin-walled structures as opposed to 3D solid elements, the numerical instability caused by the shell elements used to model the stiffeners significantly inflated the computational effort in this study (Table 4).

The effect of welding on the response curves under the uncorroded surface condition is shown in Figure 10. The welding-induced imperfections have a negligible effect on the initial, linear and post-buckling response of the panel. However, in the nonlinear stage before the ultimate load is reached, the effect of welding becomes increasingly evident as the displacement approaches D_{cr}. It has already been demonstrated that welding-induced imperfections can decrease or increase the ultimate strength of panels depending on their slenderness ratio [11]. Results in Figure 10 demonstrate that the welding has increased the ultimate strength of the panel studied herein by around 9.5%. This was found to be predominantly caused by the geometrical imperfection via a parametric study, in which the effects of residual stress, material softening, and geometrical imperfection were investigated separately.

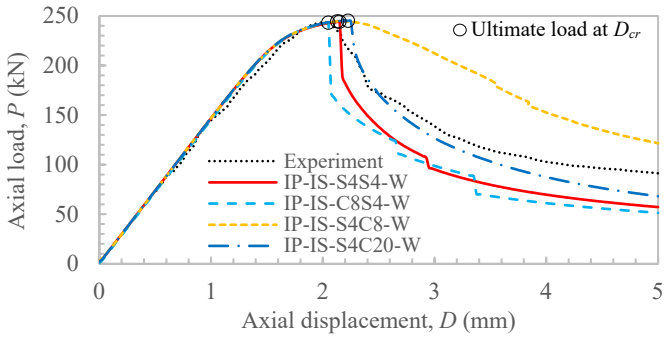

FIGURE 9: THE EFFECT OF ELEMENT TYPE USED TO MODEL THE PLATING AND STIFFENERS ON THE PANEL RESPONSE CURVE UNDER THE UNCORRODED SURFACE CONDITION.

TABLE 4: CPU TIME SUMMARY FOR THE MODELS IN FIGURE 9 BY AMD EPYC 7713 64-CORE PROCESSOR.

Model #	No. of time increments	CPU time (s) X10^5
IP-IS-S4S4-W	8219	1.8
IP-IS-C8S4-W	1942	3.8
IP-IS-S4C8-W	363	0.15
IP-IS-S4C20-W	417	0.97

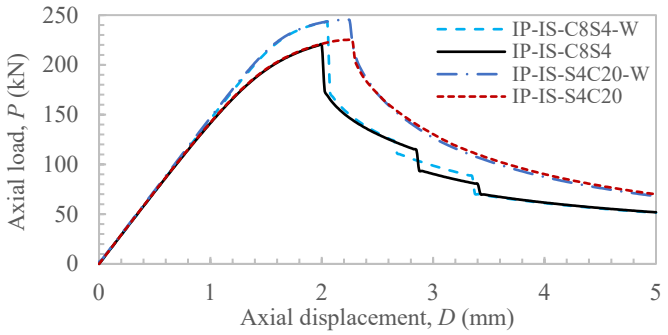

FIGURE 10: THE EFFECT OF WELDING ON THE RESPONSE CURVE UNDER THE UNCORRODED SURFACE CONDITION.

Figure 11 compares the response curves of the corroded panels with those of their uncorroded counterparts with and without the welding effects considered. In all the models, the stiffener surface condition governs the overall panel response such that when the stiffeners are intact the response curves remain almost unchanged regardless of the plating surface condition. Note that this does not mean the corroded plating does not deteriorate the panel's structural performance because the pits could still induce significant stress concentrations and reduce the fatigue life of the panel (Figure 12). Contrary to the

corroded plating condition, corroded stiffeners always reduce the overall strength of the panel during the nonlinear response in both buckling and post-buckling stages. This has caused around 10% reduction in the ultimate strength of the panel. The reduction in strength escalates in the post-buckling stage until it reaches 37% shortly after the critical displacement. Then, it gradually diminishes with displacement.

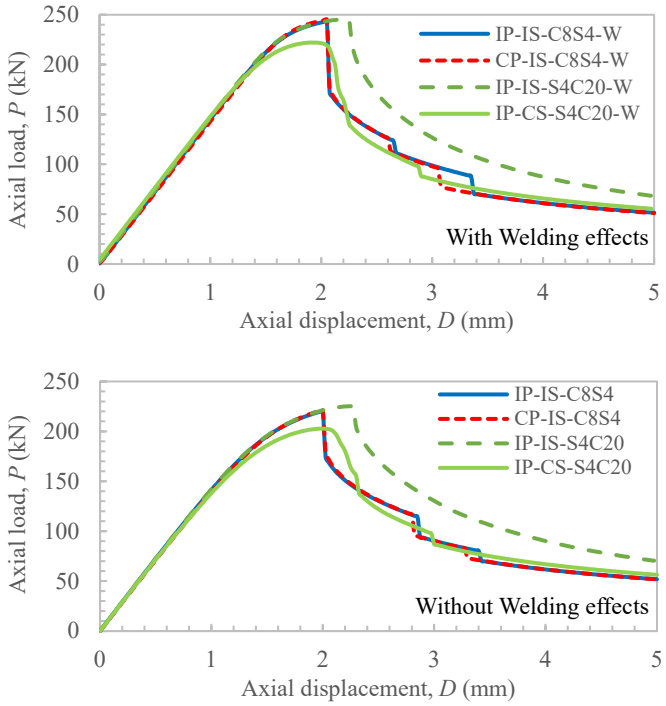

FIGURE 11: THE EFFECT OF CORROSION ON THE PANEL RESPONSE CURVE.

The stress localization at the corrosion pits significantly changed the stress distribution pattern in both the plating and stiffeners. The stress distributions in the plating and stiffeners at the critical displacement point, D_{cr}, are displayed in Figures 12 and 13. The models in these figures have no welding-induced imperfections such that the effect of pitting corrosion on the stress distribution pattern can be studied without the residual stress fields obstructing the visualization of the stress pattern induced by the corrosion damage. In Figure 12, the maximum stress in the plating at D_{cr} has increased by 50% compared to its intact condition. This increase in the maximum stress due to corrosion is smaller for the stiffeners in Figure 13 (around 12%). This is because the maximum stress in the intact stiffeners just before buckling is around 270 MPa which is their yield strength, and in the plastic regime stress elevates much lower with strain compared to the elastic phase. However, with the pitting corrosion damage applied to the stiffeners, they undergo localized plastic deformations at multiple pit sites experiencing noticeable plastic strains, up to 1.5% at D_{cr} (Figure 14). Plastic strains in the intact stiffeners at D_{cr} were negligible and thus not shown in Figure 14.

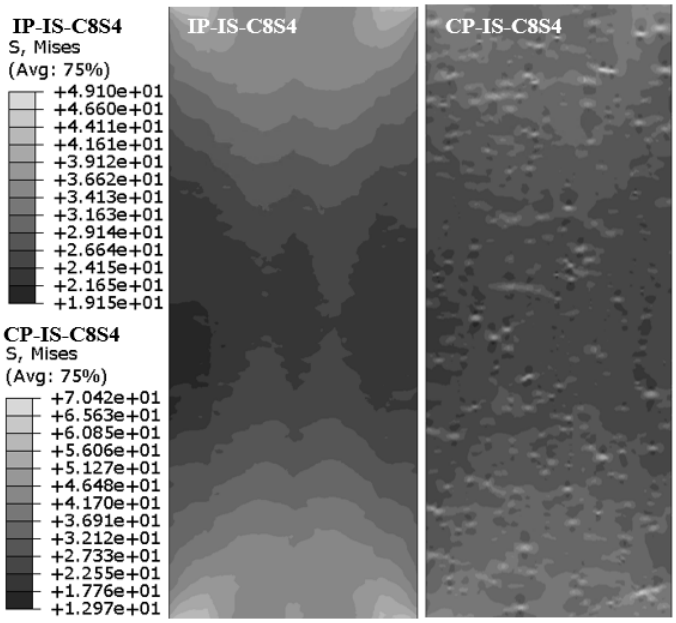

FIGURE 12: VON MISES STRESS DISTRIBUTION IN THE CORRODED PLATING (RIGHT) AND ITS INTACT COUNTERPART (LEFT) AT D_{cr} WITHOUT WELDING EFFECTS CONSIDERED.

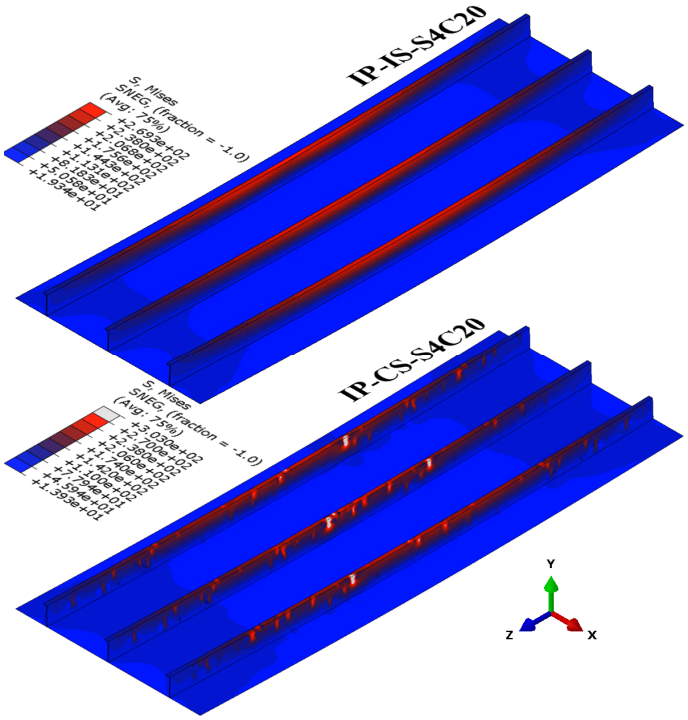

FIGURE 13: VON MISES STRESS DISTRIBUTION IN THE MODEL WITH CORRODED STIFFENERS (BOTTOM) AND ITS INTACT COUNTERPART (TOP) AT THE CRITICAL DISPLACEMENT, D_{cr}, WITHOUT WELDING EFFECTS CONSIDERED. LIGHT GREY COLOUR SHOWS THE YIELD MATERIAL.

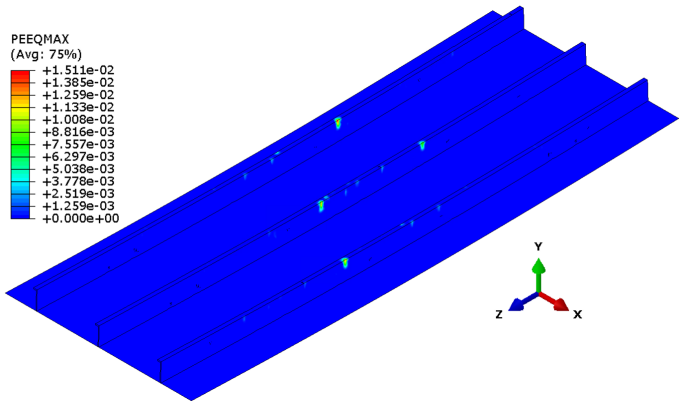

FIGURE 14: PLASTIC STRAIN DISTRIBUTION IN THE MODEL WITH CORRODED STIFFENERS AND WITHOUT WELDING-INDUCED IMPERFECTIONS, IP-CS-S4-C20, AT D_{cr}.

All investigated cases experienced a similar failure/collapse mechanism, which was initiated with the global buckling of the panel, corresponding to the onset of the nonlinear portion of the response curves in Figures 9–11. As the compressive load increased following the global buckling, the stiffeners underwent local buckling, as depicted in Figure 15, resulting in the load drop at D_{cr} in the response curves. Welding-induced imperfections and corrosion did not affect the buckling mode shapes of the panel. However, for the corroded cases, material yielding at the pit sites occurred before the ultimate load was reached as previously discussed. The presence of pitting corrosion in the stiffeners amplified local deformations, leading to sharper bendings at the local buckling zones compared to the intact models due to the thinner cross-section areas at the pit sites. Consequently, the panel with corroded stiffeners exhibited a reduction of approximately 10% in ultimate strength compared to the intact panel.

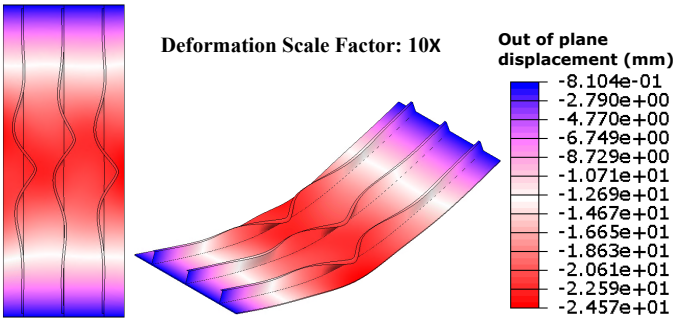

FIGURE 15: TYPICAL BUCKLING MODE SHAPE OF ALL THE CASES INVESTIGATED IN THE PRESENT STUDY IMMEDIATELY AFTER D_{cr}. THE FIGURE WAS OBTAINED FROM IP-IS-C8S4 MODEL. THE CONTOUR PLOT SHOWS THE OUT-OF-PLANE DISPLACEMENT.

4. CONCLUSION

The effect of welding-induced imperfections and pitting corrosion damage on the buckling and post-buckling behaviour of an AA6082-T6 extruded panel was studied using FEM. A mass loss of 275.77 g/m^2 due to pitting corrosion was assumed. This is equivalent to approximately 4 years of full immersion in seawater and longer under other exposure conditions. The main conclusions are as follows:

- The overall buckling and post-buckling behaviour of the panel was mainly governed by the stiffeners response. Consequently, numerical results were found to be very sensitive to the element type used to model the stiffeners. Hexahedral elements with four elements along the thickness provided significantly faster solutions as opposed to shell elements by facilitating more stable solutions. Models with quadratic hexahedral elements returned the closest correlation between the experimental and numerical post-buckling response curves.
- Since the stiffener behaviour controls the general response of the panel, pitting corrosion damage in the plating with intact stiffeners did not affect the response curve either before or after the buckling. However, it significantly changed the stress distribution in the plating such that the maximum stress was increased by 50% compared to the intact plating condition. This could significantly reduce the fatigue life of the plating.
- Pitting corrosion damage in the stiffeners reduced the ultimate strength of the panel by around 10%. The post-buckling strength was also reduced by up to 37%. Besides, multiple pit sites experienced noticeable plastic deformations before the onset of buckling while the plastic strain in the intact stiffeners before buckling was negligible.
- Welding-induced imperfections increased the ultimate strength of the panel by around 9.5%. This was found to be predominantly caused by the geometrical imperfection. However, the welding did not influence the initial, linear behaviour and the post-buckling nonlinear response of the panel.

It should be noted that the conclusions presented above are valid for the specific panel investigated in the present study and may not be generalizable to other panels with different dimensions, materials, and/or corrosion characteristics.

ACKNOWLEDGEMENTS

The financial support of the Research Council of Norway through the Centers of Excellence funding scheme, project AMOS (Grant number 223254) and the Centers for Research-based Innovation funding scheme, project CASA (Grant number 237885), at the Norwegian University of Science and Technology are acknowledged.

REFERENCES

[1] Melchers, R. E., 2015, "Time dependent development of aluminium pitting corrosion," Advances in Materials Science and Engineering.
[2] Aalberg, A., Langseth, M., and Larsen, P. K., 2001, "Stiffened aluminium panels subjected to axial compression," Thin-Walled Structures, 39(10), pp. 861-885.
[3] Rønning, L., Aalberg, A., and Kristian Larsen, P., 2010, "An experimental study of ultimate compressive strength of

transversely stiffened aluminium panels," Thin-Walled Structures, 48(6), pp. 357-372.
[4] Zha, Y., and Moan, T., 2003, "Experimental and numerical prediction of collapse of flatbar stiffeners in aluminum panels," Journal of Structural Engineering, 129(2), pp. 160-168.
[5] Rigo, P., Sarghiuta, R., Estefen, S., Lehmann, E., Otelea, S. C., Pasqualino, I., Simonsen, B. C., Wan, Z., and Yao, T., 2003, "Sensitivity analysis on ultimate strength of aluminium stiffened panels," Marine Structures, 16(6), pp. 437-468.
[6] Paik, J. K., 2009, "Buckling collapse testing of friction stir welded aluminum stiffened plate structures," Report SR-1454. Washington (DC): Ship Structure Committee.
[7] Khedmati, M. R., Zareei, M. R., and Rigo, P., 2009, "Sensitivity analysis on the elastic buckling and ultimate strength of continuous stiffened aluminium plates under combined in-plane compression and lateral pressure," Thin-Walled Structures, 47(11), pp. 1232-1245.
[8] Paulo, R. M. F., Teixeira-Dias, F., and Valente, R. A. F., 2013, "Numerical simulation of aluminium stiffened panels subjected to axial compression: Sensitivity analyses to initial geometrical imperfections and material properties," Thin-Walled Structures, 62, pp. 65-74.
[9] Li, C., Ren, H., Zhu, Z., and Guedes Soares, C., 2018, "Numerical investigation on the ultimate strength of aluminium integrally stiffened panels subjected to uniaxial compressive load," Thin-Walled Structures, 127(December 2017), pp. 221-234.
[10] Liu, B., Doan, V. T., Garbatov, Y., Wu, W., and Guedes Soares, C., 2020, "Study on Ultimate Compressive Strength of Aluminium-Alloy Plates and Stiffened Panels," Journal of Marine Science and Application, pp. 534-552.
[11] Wang, X., Amdahl, J., and Egeland, O., 2022, "Numerical study on buckling of aluminum extruded panels considering welding effects," Marine Structures, 84, p. 103230.
[12] Wang, X., and Amdahl, J., "Analysis of Welding Influences on Extruded Aluminum Panel Buckling," ASME 2022 41st International Conference on Ocean, Offshore and Arctic EngineeringV002T02A073.
[13] Liang, M., 2019, "Characterisation of pitting corrosion for aluminium alloys in natural sea-water and freshwater immersion environments," PhD dissertation. University of Newcastle.
[14] Liang, M., Chaves, I., and Melchers, R., 2016, "Long-term pitting corrosion of 6060 aluminium alloy immersed in natural seawater," Corrosion & Prevention.
[15] Zuñiga Tello, I. F., Domínguez Almaraz, G. M., López Garza, V., and Guzmán Tapia, M., 2019, "Numerical investigation of the stress concentration on 7075-T651 aluminum alloy with one or two hemispherical pits under uniaxial or biaxial loading," Advances in Engineering Software, 131, pp. 23-35.
[16] Zhang, J., Shi, X. H., and Guedes Soares, C., 2017, "Experimental analysis of residual ultimate strength of stiffened panels with pitting corrosion under compression," Engineering Structures, 152, pp. 70-86.
[17] Feng, L., Hong, K., Li, D., and Shi, H., 2022, "Ultimate torsional strength assessment of large deck opening stiffened box girder subjected to pitting corrosion," Ocean Engineering, 251, p. 111059.
[18] Feng, L., Hu, L., Chen, X., and Shi, H., 2020, "A parametric study on effects of pitting corrosion on stiffened panels' ultimate strength," International Journal of Naval Architecture and Ocean Engineering, 12, pp. 699-710.
[19] Sultana, S., Wang, Y., Sobey, A. J., Wharton, J. A., and Shenoi, R. A., 2015, "Influence of corrosion on the ultimate compressive strength of steel plates and stiffened panels," Thin-Walled Structures, 96, pp. 95-104.
[20] Wang, R., Ajit Shenoi, R., and Sobey, A., 2018, "Ultimate strength assessment of plated steel structures with random pitting corrosion damage," Journal of Constructional Steel Research, 143, pp. 331-342.
[21] Li, D., Feng, L., Huang, D., Shi, H., and Wang, S., 2021, "Residual ultimate strength of stiffened box girder with coupled damage of pitting corrosion and a crack under vertical bending moment," Ocean Engineering, 235, p. 109341.
[22] Paik, J. K., Lee, J. M., and Ko, M. J., 2003, "Ultimate compressive strength of plate elements with pit corrosion wastage," Proceedings of the Institution of Mechanical Engineers, Part M: Journal of Engineering for the Maritime Environment, 217(4), pp. 185-200.
[23] Paik, J. K., Lee, J. M., and Ko, M. J., 2004, "Ultimate shear strength of plate elements with pit corrosion wastage," Thin-Walled Structures, 42(8), pp. 1161-1176.
[24] Shi, X. H., Zhang, J., and Guedes Soares, C., 2018, "Numerical assessment of experiments on the ultimate strength of stiffened panels with pitting corrosion under compression," Thin-Walled Structures, 133, pp. 52-70.
[25] Yang, Y., Yu, Q., He, Z., Ma, J., and Qin, J., 2020, "Investigation on failure mechanism of stiffened plates with pitting corrosion under uniaxial compression," Applied Ocean Research, 102, p. 102318.
[26] Melchers, R., 2015, "On the bi-modal long-term characteristic for metallic corrosion," Proceedings conference corrosion & prevention, Adelaide, pp. 15-18.
[27] Melchers, R. E., 2018, "A review of trends for corrosion loss and pit depth in longer-term exposures," Corrosion and Materials Degradation, 1(1), pp. 42-58.
[28] Mokhtari, M., and Melchers, R. E., 2019, "Next-generation fracture prediction models for pipes with localized corrosion defects," Engineering Failure Analysis, 105, pp. 610-626.
[29] Mokhtari, M., and Melchers, R. E., "Advanced numerical method for failure assessment of corroded steel pipes," The 26th International Ocean and Polar Engineering Conference, Rhodes, Greece, June 2016.
[30] Mokhtari, M., and Melchers, R. E., 2018, "A new approach to assess the remaining strength of corroded steel pipes," Engineering Failure Analysis, 93, pp. 144-156.
[31] Mokhtari, M., and Melchers, R. E., 2020, "Reliability of the conventional approach for stress/fatigue analysis of pitting corroded pipelines – Development of a safer approach," Structural Safety, 85, p. 101943.
[32] Dassault Systèmes 2019, "SIMULIA User Assistance, Abaqus."

[33] Xu, S.-h., and Wang, Y.-d., 2015, "Estimating the effects of corrosion pits on the fatigue life of steel plate based on the 3D profile," International Journal of Fatigue, 72, pp. 27-41.
[34] Mokhtari, M., Wang, X., and Amdahl, J., 2023, "Numerical analysis of pit-to-crack transition under corrosion fatigue using a stochastic pit generation algorithm," Advances in the Analysis and Design of Marine Structures. J. W. Ringsberg, and C. Guedes Soares, eds., CRC Press. doi.org/10.1201/9781003399759-55.